Miniature Soft Robot for Enhanced Gastrointestinal Navigation and Diagnostics

Dana Hsu
Mechanical Engineering
University of Washington
Seattle, USA
danahsu@uw.edu

Kao Cheng Liu
Mechanical Engineering
University of Washington
Seattle, USA
kliu0220@uw.edu

Woody Pan
Mechanical Engineering
University of Washington
Seattle, USA
cp8761@uw.edu

Zi Ye
Mechanical Engineering
University of Washington
Seattle, USA
yez24@uw.edu

***Abstract*—This paper introduces a novel soft robot design, particularly suitable for gastrointestinal (GI) tract navigation. Inspired by a stent-shaped robot initially intended for arterial movement [1], this innovative design has been modified and scaled for use within larger anatomical structures, specifically the small and large intestines. The robot, made with a uniform magnetization and neodymium-iron-boron (NdFeB) for magnetic actuation, features a hollow cylindrical lattice structure to accommodate an optical device, augmenting its diagnostic capabilities. This paper outlines the robot's theoretical analysis, design specification, and fabrication process, which involves an integrated mold production and precise micro-drilling techniques, along with the implementation of a uniform magnetic field for effective control via an external robotic arm.**

Keywords—MEMS device, soft robot, gastrointestinal navigation, stent-shaped robot, colonoscopy

I. INTRODUCTION

Traditionally, colonoscopy can only access the large intestine, and while capsule endoscopy eliminates the need for fiber optic cables, it lacks the ability to control the direction of the capsule once inside the body. Although there are soft robots capable of navigating the large intestine [2], they do not possess endoscopic capabilities. Our soft robot overcomes these limitations, not only addressing the constraint of conventional colonoscopy that restricts access to only the large intestine but also providing the ability to control the direction of the soft robot within both the large and small intestines. This innovative design broadens potential application scopes and has significant implications for future developments in the field.

II. STENT-SHAPED WIRELESS ROBOT

A. Design Parameters

The proposed robot aims to achieve shape adaptation for various diameters in both the large and small intestines, enabling it to navigate through these anatomical structures. It should be capable of performing forward and backward movement and anchoring itself within the intestine without causing any damage. To meet these requirements, we have chosen a stent-shaped wireless robot initially designed by Wang et al.[1] for arterial movement, and we have modified and scaled it up for intestinal applications.

To enable effective locomotion and radial deformation, the robot has been designed as a cylindrical hollow stent with uniform magnetization. The body of the robot incorporates NdFeB, a magnetic material that facilitates magnetic actuation. The dimensions of the robot have been adjusted proportionally based on the differences in artery and intestine diameters. Considering previous studies [3], we based our design on the dimensions of the small intestine, specifically the jejunum, which has the largest mean diameter of approximately 3 cm. Additionally, existing gastrointestinal stents commonly have a diameter of 30 mm and a length of 10 cm [4].

In our work, we scaled up most of the original design by Wang et al. by a factor of 20. This scaling includes a four-fold increase in the thickness of the wall, resulting in a radial force that is approximately 64% of the original design. However, further experiments are necessary to obtain precise data and validate the actual performance of the scaled-up design. Design parameters of the robot are shown in TABLE I.

TABLE I
DESIGN PARAMETERS OF THE ROBOT

Parameters	Original design	Our design
Strut spacing h (mm)	0.4	8
Radius of curvature at the crown junction ρ (mm)	0.3	6
Axial amplitude of each segment f (mm)	0.5	10
Overall length l_r (mm)	5	100
Initial diameter ϕ_r (mm)	1.5	30
Wall thickness t_r (mm)	0.3	1.2
Coated helix pitch p_r (mm)	0.5	10
Helical angle φ (deg)	8	8
Young's modulus E_r (MPa)	6.44 ± 1.1	6.44 ± 1.1

B. Structure of Soft Robot

The structure of our soft robot is primarily composed of a hollow cylindrical lattice with an open end, which is patterned in a diamond hexagonal design(Fig.1a,1b,1c). Due to the inclusion of magnetic particles in the fabrication material of the cylinder, this lattice cylinder exhibits a uniform magnetic field. This uniform magnetic field enables external robotic arms to effectively control our soft robot. To allow autonomous movement of the soft robot within the large and small intestines, we employ Polymethylsiloxane (PDMS) in mass ratio 12:1 along with Neodymium-Iron-Boron particles. This allows the soft robot to freely expand and contract within intestinal tubes ranging in diameter from 2 centimeters to 3 centimeters.

To enable our soft robot to accommodate an optical device of 2.5mm, the robot's front end is similarly sealed with the same structure as hollow cylindrical lattice, leaving only a hole of approximately 1.5mm. The structure around the hole possesses significant elasticity, facilitating the insertion of the optical device press fit into the 1.5mm hole and securing it firmly in place. The optical device's fiber optic cable can be routed from the cylinder's rear end, without affecting the overall structure of the soft robot.

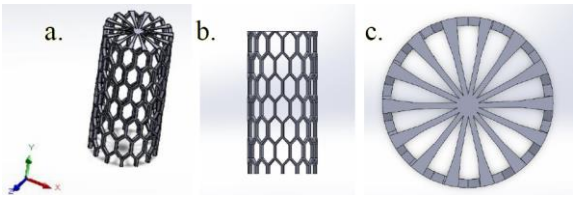

Figure 1. The structure of the soft robot. a. The whole view of the soft robot. b. The side view of the soft robot. c. The top view of the soft robot.

C. Dynamics

The proposed system includes a rotational cubic NdFeB permanent magnet mounted on a 7-DoF robotic arm, enabling three-dimensional magnetic actuation. To assess the feasibility of the setup and understand the robot's movement capabilities, we analyzed the dynamics of the system.

The force acting on the robot is influenced by two factors: friction F_{fric} and magnetic force F_{mag}. The dynamics of the robot during locomotion can be effectively modeled as follows:

$$F_{mag,y} + F_{fric,\perp}\, cos\cos(\varphi) - F_{fric,\parallel}\, sin\sin(\varphi) = m_r \ddot{\omega}_y \quad (1)$$

$$T_{mag,y} - ((F_{fric,\parallel}\, cos\cos(\varphi) + sin\, F_{fric,\perp}\sin(\varphi))R_d = J_y \quad (2)$$

Where,

$F_{fric,\perp}$: frictional forces perpendicular to helix structure

$F_{fric,\parallel}$: frictional forces parallel to helix structure

φ: helix angle

m_r: robot mass

ω_y: robot displacement along the y-axis

R_d: robot radius after radial deformation

J_y: moment of inertia around the y-axis

θ_y: rotation angle of the robot around the y-axis

The radial force can be expressed as

$$F_n = 10\frac{3E_r I_b \Delta l_c}{l_b^3} tan\left(\frac{\pi}{3}\right) \quad (3)$$

Where,

F_n: radial force

E_r: Young's modulus of the robot material

I_b: second moment of area for the cross-section of a single beam

Δl_c: change in distance of the two facing beams of the cell under deformation

l_b: length of the single beam

Determining the exact coefficient of friction between the robot and the intestine wall requires conducting experiments due to the presence of mucosa, which can significantly affect the frictional properties. It is important to note that the coefficient of friction between the robot and the intestine wall is generally higher than the coefficient of friction between the robot and the artery wall.

To make reasonable assumptions in the absence of experimental data, we assume that the coefficient of friction between the robot and the intestine wall is ten times greater than the coefficient of friction between the robot and the artery wall.

Additionally, the magnetization of a material follows the following relationship:

$$M = \chi H \quad (4)$$

Where,

M: magnetization

χ: magnetic susceptibility

H: field intensity

We also have:

$$M = \frac{m}{V} \quad (5)$$

Where,

m: magnetic moment

V: volume

Since the material remains the same, the magnetic moment m is proportional to the volume V of the magnet. In our design, the volume of the robot is approximately 1920 times larger than the volume of the original design. Consequently, the magnetic moment is also approximately 1920 times larger.

The formulas for magnetic force and magnetic moment applied on the robot are as follows:

$$F_{mag,y} = (m \cdot \nabla)B \quad (6)$$

$$T_{mag} = m \times B \quad (7)$$

Where,

$F_{mag,y}$: magnetic force along the y-axis
$T_{mag,y}$: magnetic torque along the y-axis
B: magnetic flux density generated by the actuation magnet

From Equation (6) and Equation (7), both $F_{mag,y}$ and the $T_{mag,y}$ are proportional to m. Since the magnetic moment is approximately 1920 times larger in our design compared to the original design, both $F_{mag,y}$ and $T_{mag,y}$ will also be approximately 1920 times larger.

Considering that $F_{mag,y}$ and $T_{mag,y}$ are significantly larger than the frictional forces $F_{fric,\perp}$ and $F_{fric,\parallel}$, it can be inferred that the robot should remain controllable under the same robotic arm setup. The increased magnetic forces and torques contribute to enhanced maneuverability and control over the robot's movement within the intestine.

D. Optical component

The structure shown in Figure 2 depicts a detailed representation of the optical component within the system. The system itself consists of two essential lenses: a stationary objective lens and a light guide lens. These lenses both incorporate thin film Fresnel lenses that can be fabricated through the MUMPs process. The size of objective lens and light guide lens is around 1 mm and 0.8 mm respectively. The entire component is around 2.5 mm in diameter. The nominal Fresnel lens size is approximately 1 mm [5]. Our intention is to minimize the optical component size to allow more space for other components.

The objective lens, which remains fixed in its position, is equipped with an image sensor situated behind it. This arrangement allows the lens to capture and process images effectively. Besides, the light guide lens is designed to facilitate the transmission of light. It is accompanied by an illumination fiber positioned at its rear, which serves the purpose of providing adequate illumination for the system.

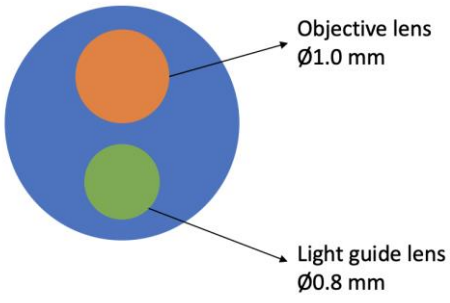

Figure 2. optical device with objective lens and light guide lens

III. FABRICATION PROCESS

To enhance the structural strength of the soft robot, we adopt an integrated mold manufacturing method, as shown in Figure 3. Initially, a positive mold is created using 3D printing, followed by the production of a negative mold using Polymethylsiloxane (PDMS). The material used for injection into the mold is a uniform mixture of PDMS at mass ratio of 12:1 and Neodymium-Iron-Boron (NdFeB), with the mass ratio of PDMS to NdFeB being 1:4. These materials are all biocompatible. Furthermore, before injecting the material into the mold, a stainless pin with a diameter of 2.76cm is placed at the exact center of the mold. This results in a hollow cylindrical lattice with an open end, which is patterned in a diamond hexagonal pattern. Following the demolding process, to augment the precision of the hole, we decided to employ a micro-drilling CNC machine to create a hole of 0.05 mm diameter at the center point of the sealed cylinder end. This hole is designated for the positioning of the optical device. Micro-drilling was chosen over laser drilling to prevent thermal damage that could potentially lead to the melting and deformation of the surrounding material during the drilling process.

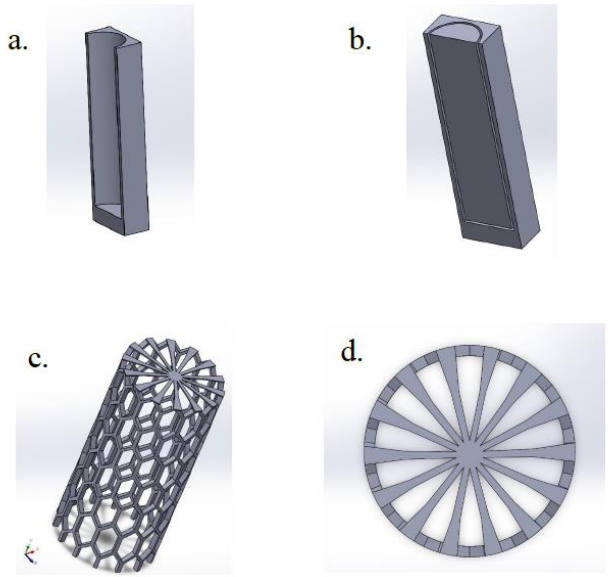

Figure 3. Fabrication of a soft robot. a. A negative mold is created. b. Injecting the material into the mold. c. Demolding. d. Micro-drilling CNC machine to create a hole.

To establish a uniform magnetic field within the soft robot, the completed robot is placed into a vibrating sample magnetometer to generate a 1.8 Tesla magnetic field, facilitating the robot's coordination with an external robotic arm.[1]

IV. APPLICATION

The innovative stent-shaped wireless soft robot provides an intriguing prospect for improved gastrointestinal (GI) tract procedures. Its exceptional design characteristics and potential for optical device integration suggests a multitude of applications. Its hollow cylindrical lattice structure might enhance disease diagnosis, offering possibly superior image resolution than current endoscopy methods, with a potential for detecting overlooked lesions. The robot could also serve as a precise delivery system for GI tract targeted therapies, potentially improving treatment effectiveness while reducing patient's discomfort. Further modifications could facilitate the detection and removal of polyps by adding a working channel on the optical component. In instances of GI bleeding, the robot might assist in diagnosing and possibly controlling the bleeding through targeted treatments or potentially add a section channel onto the device. Finally, the robot could act as a useful educational tool, providing an interactive view of the GI tract through real-time, high-resolution imaging. Nevertheless, exhaustive in vitro and in vivo testing is needed to ensure safety, reliability, and efficacy. Navigating the regulatory approval processes is an additional consideration that may necessitate substantial time and resources.

V. CONCLUSION

In summary, this study introduces a novel soft robotics design utilizing the medical diagnostic and navigation field. We adapt a stent-shaped robot for intestinal applications, integrating uniform magnetization and the magnetic material NdFeB to optimize locomotion and radial deformation. The design features a soft hollow and stented-shape cylindrical lattice fabricated through the molding process, that accommodates an optical component, potentially revolutionizing endoscopic procedures.

The fabrication of the main soft body is a combination of molding and micro-drilling techniques. Though the theoretical analysis of the robot's dynamics and modeling design specification are comprehensively discussed, the necessity for further experimental validation is emphasized, given the intricacy of friction dynamics within the GI tract.

This work marks an innovation in biomedical navigation, underlining the transformative potential in clinical diagnostics and treatments. Future research will focus on optimizing the robot's dimensions and material properties to enhance control and patient comfort.

VI. ACKNOWLEDGMENT

This work is supervised by Professor Karl F. Böhringer from University of Washington. Many thanks for his guidance and continuous support.

REFERENCES

[1] T. Wang *et al.*, "Adaptive wireless millirobotic locomotion into distal vasculature," *Nature Communications*, vol. 13, no. 1, p. 4465, Aug. 2022, doi: https://doi.org/10.1038/s41467-022-32059-9.

[2] K. E. Peyer, L. Zhang, and B. J. Nelson, "Bio-inspired magnetic swimming microrobots for biomedical applications," *Nanoscale*, vol. 5, no. 4, pp. 1259–1272, 2013, doi: https://doi.org/10.1039/c2nr32554c.

[3] H. F. Helander and L. Fändriks, "Surface area of the digestive tract – revisited," *Scandinavian Journal of Gastroenterology*, vol. 49, no. 6, pp. 681–689, Apr. 2014, doi: https://doi.org/10.3109/00365521.2014.898326.

[4] H. J. Chun, E. S. Kim, J. J. Hyun, Y. D. Kwon, B. Keum, and C. D. Kim, "Gastrointestinal and biliary stents," *Journal of Gastroenterology and Hepatology*, vol. 25, no. 2, pp. 234–243, Feb. 2010, doi: https://doi.org/10.1111/j.1440-1746.2009.06152.x.

[5] E. Arbabi, A. Arbabi, S. M. Kamali, Y. Horie, M. Faraji-Dana, and A. Faraon, "MEMS-tunable dielectric metasurface lens," *Nature Communications*, vol. 9, no. 1, Feb. 2018, doi: https://doi.org/10.1038/s41467-018-03155-6.